PCCP

Accepted Manuscript

ROYAL SOCIETY OF CHEMISTRY

www.rsc.org/pccp

Journal Name

RSCPublishing

ARTICLE

Anomalous Partitioning of Water in Coexisting Liquid Phases of Lipid Multilayers near 100% Relative Humidity

Cite this: DOI: 10.1039/x0xx00000x

Yicong Ma[a], Sajal K. Ghosh[a,*], Sambhunath Bera[a,**], Zhang Jiang[b], Christian M. Schlepütz[b], Evguenia Karapetrova[b], Laurence B. Lurio[c] and Sunil K. Sinha[†a]

Received 00th January 2012,
Accepted 00th January 2012

DOI: 10.1039/x0xx00000x

www.rsc.org/

Ternary lipid mixtures incorporating cholesterol are well-known to phase separate into liquid-ordered (Lo) and liquid-disordered (Ld) phases. In multilayers of these systems, the laterally phase separated domains register in columnar structures with different bilayer periodicities, resulting in hydrophobic mismatch energies at the domain boundaries. In this paper, we demonstrate via synchrotron-based X-ray diffraction measurements, that the system relieves the hydrophobic mismatch at the domain boundaries by absorbing larger amounts of inter-bilayer water into the Ld phase with lower d-spacing as the relative humidity approaches 100%. The lamellar repeat distance of the Ld phase swells by an extra 4 Å, well beyond the equilibrium spacing predicted by the inter-bilayer forces. This anomalous swelling is caused by the hydrophobic mismatch energy at the domain boundaries, which produces a surprisingly long-range effect. We also demonstrate that the d-spacings of the lipid multilayers at 100% relative humidity do not change when bulk water begins to condense on the sample.

INTRODUCTION

As model systems of biological membranes, lipid multilayers exhibit a rich variety of structures and phase equilibria due to an intricate interplay between different intrabilayer and interbilayer forces. Lipid multilayers are commonly used as model systems for X-ray and neutron scattering structural studies. A repeated lamellar spacing (d-spacing) is usually measured. For lipid bilayers with neutral charge, the water layer thickness between the bilayers is determined mainly by the van der Waals interaction, hydration forces and Helfrich repulsion [1]. There are different ways of changing the water content by manipulating the repulsive undulation force [2], such as adding salt to the aqueous solution [3–6] and changing bilayer material to change the curvature elasticity [7,8]. The substrate effects also suppress the undulation for several bilayers close to the solid support [9,10]. Differences in membrane dynamics based on substrate effects have also been studied using fluorescence microscopy [11–16].

Since Hønger *et al*. reported the phenomenon of anomalous swelling of lipid bilayers near the main transition temperature in 1994 [17], there has been much attention paid to this phenomenon [18–24]. This extra swelling is explained by the sudden softening of the membrane when crossing the main transition temperature, which increases the undulation and Helfrich repulsion. The effect is lipid dependent, e.g., a typical anomalous swelling for 1,2-dimyristoyl-sn-glycero-3-phosphocholine (DMPC) is about an extra 2Å increase in the water thickness at the main transition [24].

In this article, we report another type of anomalous swelling, which is not related to the phase transition, but rather due to the pure geometrical effect of domain boundaries. This novel phenomenon is discovered in phase-separated mixed lipid multilayers, in which the interlayer coupling plays an important role in the columnar order of registered domains as reported in our earlier research [25]. The phase separation in model ternary mixture lipid systems has been studied extensively following the work of Veatch and Keller on phase diagrams [26–29]. In previous work [25], we have shown that when the ternary mixture is made into a multilayer, the phase separated domains in each bilayer would couple with domains of the same phase in neighboring bilayers through the interlayer coupling interactions. This coupling is a long range effect, which leads to columnar order crossing hundreds of bilayers, basically across the whole sample.

To interpret those results, we postulated a layered structure according to the deduced electron density profiles from the X-ray measurements of the multilayers under partial hydration (a relative humidity (RH) around 96~98%), where the water layer thicknesses in the different phases are very similar, therefore the hydrophobic mismatch energy is accumulated at the domain boundaries. In this study, we demonstrate that when the system gradually approaches full hydration, a super

swelling state, or a pseudo-unbinding state of the L_d phase occurs in order to adjust for the boundary mismatch energy (as depicted in Figure 1).

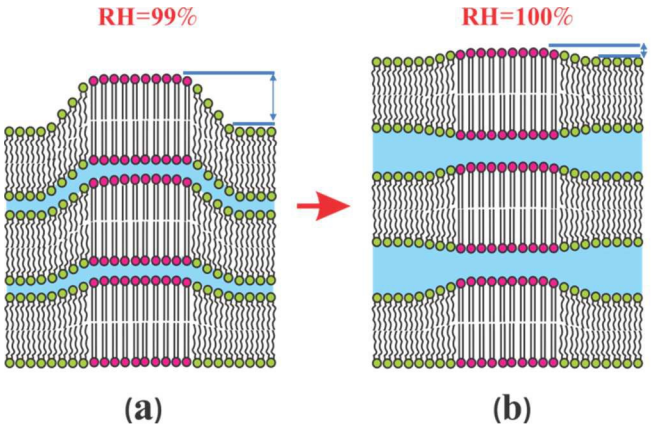

FIG. 1. Schematic drawing of the lipid multilayer structure at partial hydration (a) and full hydration (b). At 99% RH, the system stacks up with similar water layer thickness (blue) for the Lo phase (red) and Ld phase (green), while at 100% hydration, , the water in the Ld phase swells to make up for the lipid length difference, therefore a pearl-shaped water layer structure forms across domains.

MATERIALS AND METHODS

I. Materials

1,2-dipalmitoyl-sn-glycero-3-phosphocholine (DPPC), 1,2-dioleoyl-sn-glycero-3-phosphocholine (DOPC) were purchased from Avanti Polar Lipids, Inc. (Alabaster, AL, USA). Cholesterol was purchased from Sigma Chemicals (St. Louis, MO, USA). The chemicals were used without further purification. The phospholipids and cholesterol were mixed in the desired proportions (1:1 DOPC:DPPC with 16% cholesterol) dissolved in chloroform and Tetrafluoroethylene (TFE) 1:1 mixture solvent [30], with a final concentration of 8mg/mL.

Silicon substrates were cut to 17 mm by 20 mm wafers, sonicated for 15 min in methanol, 15 min in miliQ water, nitrogen dried, followed by 15 min UV cleaning under a UV lamp to make the surface hydrophilic. The prepared substrates were placed on a carefully leveled platform for lipid deposition. 150 µL of lipid solution were deposited on each substrate and immediately covered by a large Petri dish for slow evaporation in the fume hood. 3~4 hours later, the samples were transferred to a vacuum chamber for 36 hours to remove any remaining traces of solvent. After removing from the vacuum, the samples were placed in humidity chambers with 96% relative humidity (RH) at 50 C to incubate for 2 days.

After they had cooled down to room temperature, the samples would phase separate into 2 different phases and interlayer domains would register across bilayers [25,31]. This registering process takes a few days to complete under partial hydration, but is much faster at 100% RH. The diffraction measurements were taken after the registering process was mostly complete.

II. X-ray diffraction and humidity control

The X-ray measurements were taken on the diffractometer at sector 33 BM at the Advanced Photon Source, Argonne National Laboratory with a 20 keV X-ray beam. Data were taken with a Pilatus 100K photon-counting area detector, which was kept at a fixed position while the sample was rotated for diffraction measurements.

The humidity chamber used was described in our previous research [32]. The chamber uses fine control of the temperature between the reservoir and the sample to control sample humidity. The chamber is extremely accurate at close to 100% RH, as demonstrated in our previous paper and also in this work. By translating the calibrated temperature differential dT to RH, we get the RH reading for our work here. Microscope measurements and d-spacing measurements at RH saturation both prove the accuracy of the method.

RESULTS

I. X-ray diffraction experiment

The multilayer being studied here was composed of 1:1 DOPC : DPPC with 16% cholesterol. At 28 °C, the system is phase separated into a liquid-ordered (L_o) phase and a liquid-disordered (L_d) phase and forms columnar order across the sample. Using the accurate humidity control setup we developed in previous studies [32] which controls the sample RH via tuning the temperature differential between the sample and the reservoir (which we denote by dT), we measured the hydration response of the multilayer using X-ray diffraction. The sample temperature was kept constant at 28 °C, while the reservoir temperature was raised to provide dT. The sample is in Lo/Ld phase coexistence, as shown in the phase diagram by Marsh [33]. The data are shown in the Figure 2 as a 3D waterfall plot.

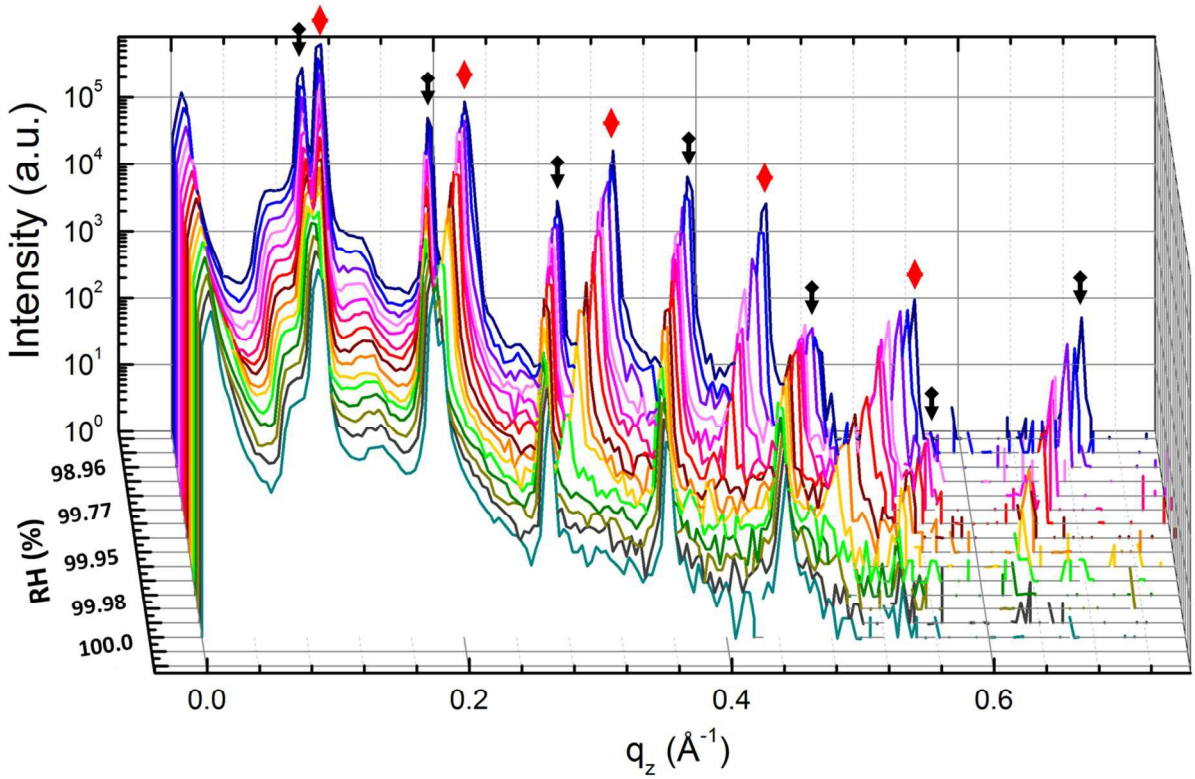

FIG. 2. X-ray diffraction data of a multilayer consisting of 1:1 DOPC : DPPC with 16% cholesterol for different RH. The RH increases from 98.96% for the top curve in black, to 100% for the bottom curve in teal. The red diamond arrows mark the diffraction peaks associated with Ld phase, while the black double arrows mark the Lo phase.

In Figure 2, we can see that with RH increasing from 98.96% (top curve in black) to 100% RH (bottom curve in teal), the two sets of distinct Bragg peaks gradually merge together. The lamellar spacing is calculated as $2\pi n/q_B$, where n is the order number of the Bragg peak and q_B is the Bragg peak position. As the Bragg peaks of the two phases start merging together, the d-spacings get closer to one another. In our calculation of d-spacings, we mainly use the n=3 order Bragg peak.

An optical microscope was mounted in the sample chamber to monitor the sample surface morphology during the X-ray diffraction experiment. As shown in Figure 3, the vertical yellow lines on the optical images marks the X-ray beam illuminated area (the footprint), while the yellow cross in the middle marks the X-ray beam center. Optical images (a)~(h) were taken at the same time while the d-spacings (a)~(h) were measured individually between 98.96% RH to 100% RH. The highly accurate high humidity control worked extremely well: as the d-spacing saturates and indicates 100% RH (as marked by the blue dashed line). The optical image shows small water droplets condensing on the sample surface when 100% RH is reached (h). Beyond this, we continue to increase the temperature differential to condense more water on the sample surface, which can be visualized in optical images (i)~(k) , when (k) shows the whole sample is covered by water. The d-spacing measured after 100% RH stayed the same after bulk water condensed on the sample, which demonstrates that the "water vapor paradox" does not exist.

During the process of more than 10 hours, the sample was stable the whole time.

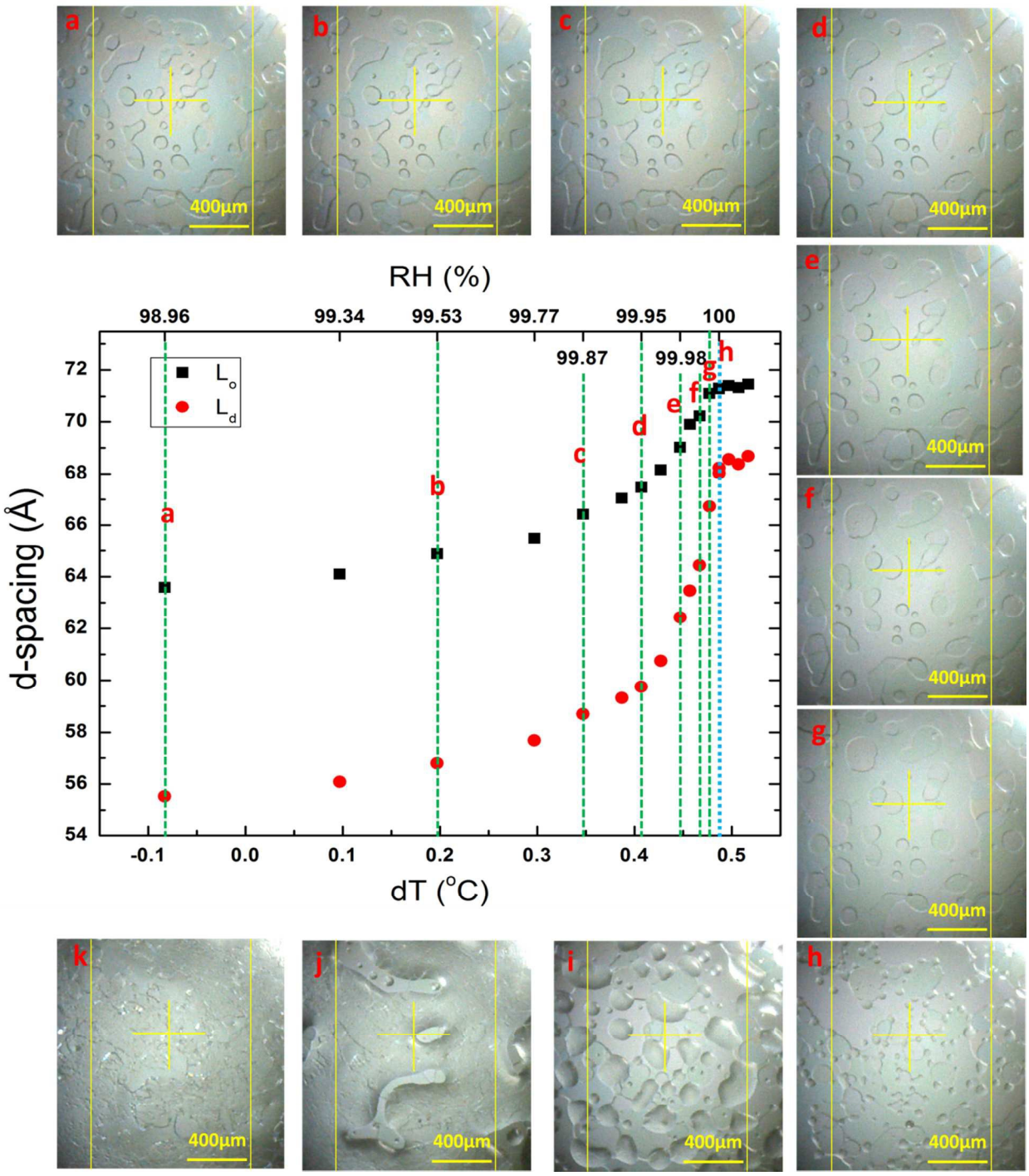

FIG. 3. d-spacing vs. temperature differential (bottom axis) and RH (top axis) plot of both Lo and Ld phase (middle plot) and optical microscopic pictures of the sample surface morphology (surrounding pictures). The RH increases from (a) 98.96% to (h) 100%, and stays 100% while increasing the temperature differential to continue condensing water on the sample (i),(j), and finally the sample is all covered with water (k).

The approximately circular features shown on the sample surface (Figure 3 (a)~(g)) were identified as L_o phase domains from our fluorescence microscopy measurements (see Supplementary material Figure S1). The contrast in the optical images is the result of the sample surface morphology, in other words, the surface height differences between the L_o and L_d phases. Also the color contrast (light pink vs. green) comes from the Newton ring effect on different film thicknesses. When comparing image (a) to image (g), one can see that the height difference between the two phases decreases dramatically from (a) to (g), while the sudden change happens around (e), which can be traced back to the accelerated rate of increase of the d-spacing around (e) in the

center plot. Somewhere between (d) and (e), the d-spacing of the L_d phase starts to swell anomalously.

II. Electron density profile (EDP) construction

In order to understand the change in d-spacing, we need to construct the relative electron density profile (EDP) for each hydration condition. EDPs are constructed from the integrated intensities of the Bragg peaks with the following equation [34]:

$$\rho_{\text{relative}}(z) = \frac{2}{d}\sum_{n} v(n)\sqrt{nI_n}\cos\left(\frac{2\pi nz}{d}\right) \quad (1)$$

where d is the lamellar spacing, $v(n)$ is the phase factor for the nth order reflection, I_n is the integrated intensity of the nth order Bragg peak. The factor $\sqrt{n}$ arises from the Lorentz correction of q_z^{-1} applied to the raw intensities I_n.

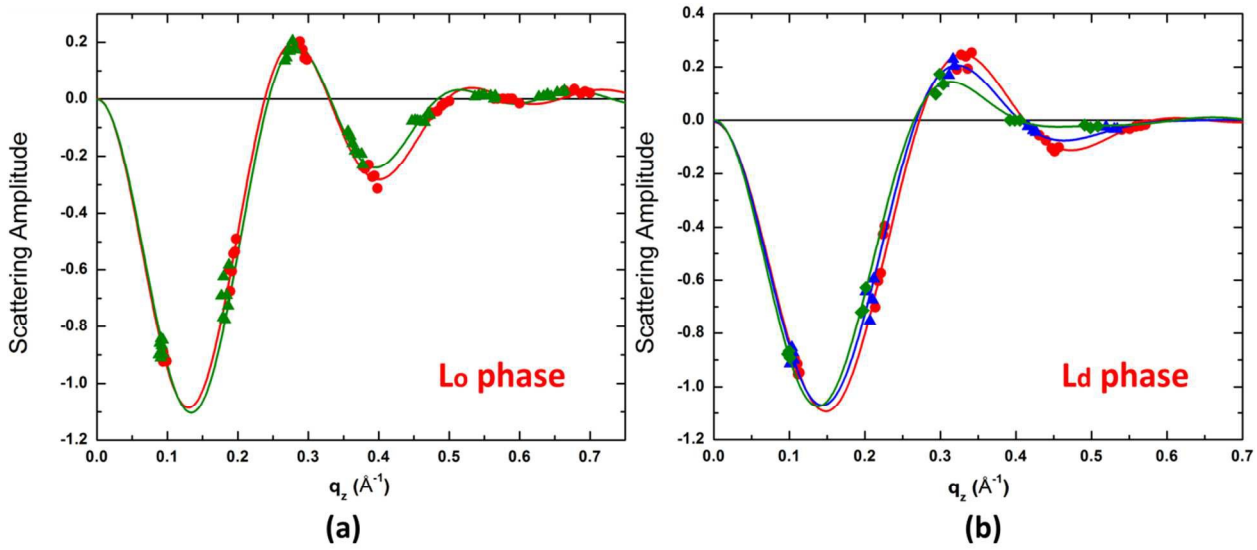

FIG. 4. Phasing diagram for Lo phase (a) and Ld phase (b). The scattering amplitudes are sampling the slightly shifted Fourier transform of the bilayer EDPs relative to water due to the bilayer form factor changes resulted from the increased fluctuations in the membrane. The increase in fluctuation is greater in the Ld phase (b) than in the Lo phase (a), as DOPC has a smaller bending modulus than DPPC. The different color lines are to demonstrate the shifting of form factor, which are fitted to the groups of scattering amplitude data points at the adjacent RH of the same color.

The correct choice for the combination of phase factor $v(n)$ is essential for the correct EDP construction. The swelling method [35] is the most commonly used method to determine the phases. Normally, diffraction data from 3 or 4 different but closely spaced hydration conditions are used to determine the phases accurately assuming the bilayer structure remains constant while swelling at partial hydration [36,37]. In our case, measurements were carried out under a range of conditions close to full hydration, and the changes with d-spacing are dramatic. When plotting the scattering amplitudes (Figure 4), we can see that they do not fall on a single smooth curve of the Fourier transform of the bilayer EDP relative to water. Thus the bilayer structure must have changed during the swelling process [38]. However, the structure change must be continuous, so that the scattering amplitudes can be fitted with slightly shifted form factors for each of the several continuous conditions. The change in form factor is due to the increased fluctuations of the bilayers [39–42]. The hydration increase close to 100% RH increases the fluctuations in the membrane, and therefore smears the form factor of the bilayer. When comparing between the L_d phase (Figure 4(b)) and the L_o phase (Figure 4(a)), we can see that the form factor shift in the L_d phase (3 fitting curves, corresponding to RH 98.96 % to 99.77%; 99.87% to 99.95 %; and 99.97% to 100 % respectively) is more than in the L_o phase (2 fitting curves, corresponding to RH 98.96% to 99.91%, and 99.95% to 100% respectively), which agrees with the fact that the L_d phase membrane (DOPC-rich) is much softer than that of the L_o phase (DPPC-rich). The phase factor choice for each order is +1 if above zero or -1 if below zero, as can be read out from Figure 4.

After the correct choices for the phase factors are made, we can construct the EDPs for each phase. Figure 5 shows the constructed EDPs for L_o (a) and L_d (b) phases, with RH increasing from the bottom curve to the top. The L_o phase EDPs are all reconstructed from 7 orders of Bragg peaks, while the L_d phase EDPs are constructed from 5 orders of Bragg peaks, except the top two dotted curves close to full hydration where only 3 orders of Bragg peaks are left present. The loss of the higher order peaks for the DOPC rich phase due to fluctuations at full hydration agrees with our previous result on pure DOPC [32]. It is evident that although the EDPs continue to smear out with increasing hydration, the bilayer thicknesses stay the same: the phosphate-to-phosphate distances (PtP) do not change during swelling, as marked with the vertical dotted green line. The cholesterol incorporated into the L_o phase is clearly evident in the EDPs, while the much smaller amount incorporated into the L_d phase is not so evident.

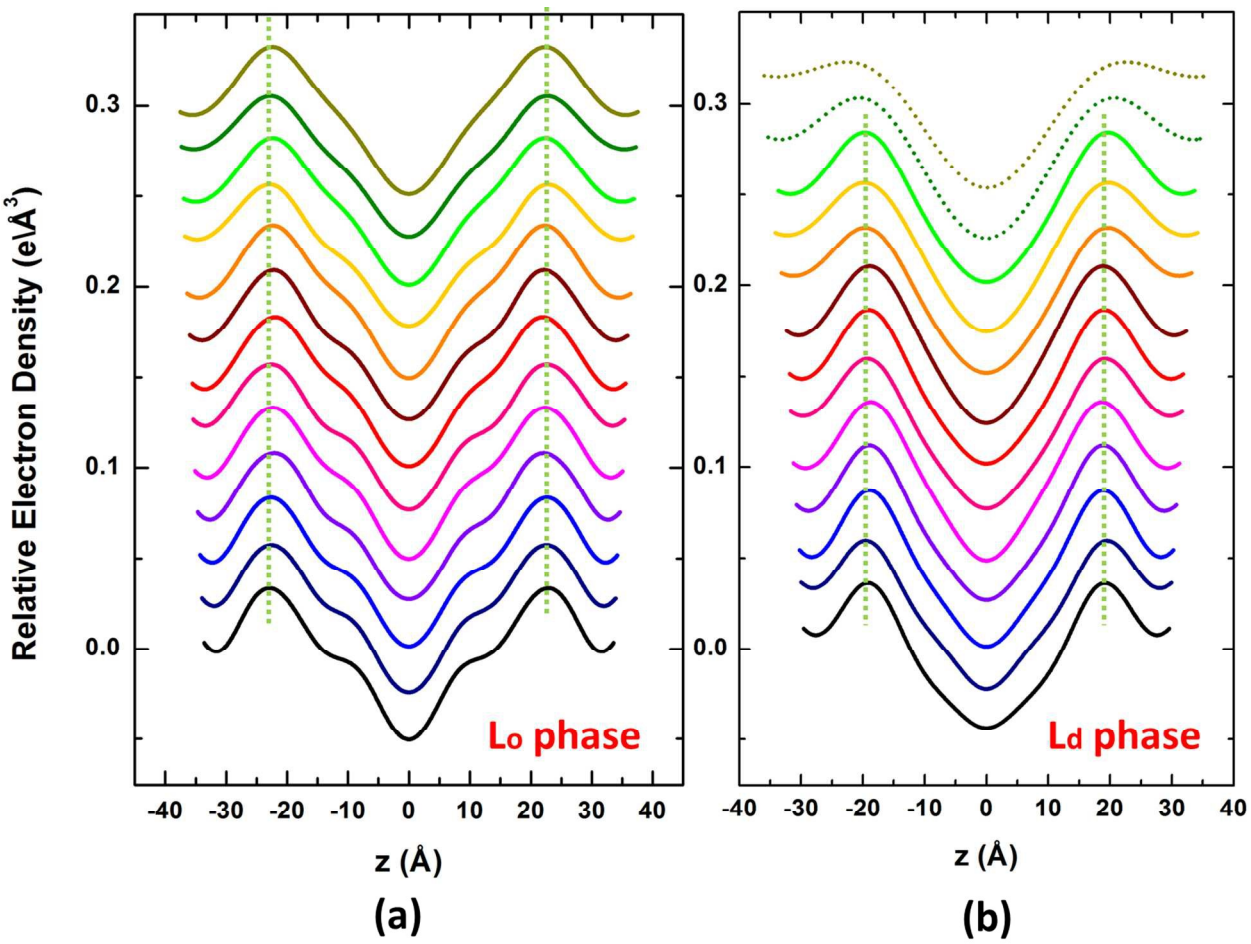

FIG. 5. Relative EDPs of Lo phase (a) and Ld phase (b), shifted for clarity. RH ranges from 98.96% for the bottom curve to 100% for the top curve. The vertical green dotted lines mark the center of the headgroup positions, which do not change with hydration. The top 2 dotted EDP curves of (b) are constructed with 3 orders of Bragg peaks, which give less resolution for the bilayer structure.

III. Anomalous swelling type II

As shown in Figure 6(a), the PtP distances for each phase are fairly constant with some small variations. Taking the average values of 44.8 Å and 38.4 Å for the PtP distances of the L_o phase and the L_d phase respectively, we can calculate the water layer thickness from the measured d-spacings:

$$d_{water} = d - PtP - 10 \qquad (2)$$

where 10 Å is a good estimate of the headgroup size [43]. The resulting water layer thicknesses d_{water} are plotted in Figure 6(b).

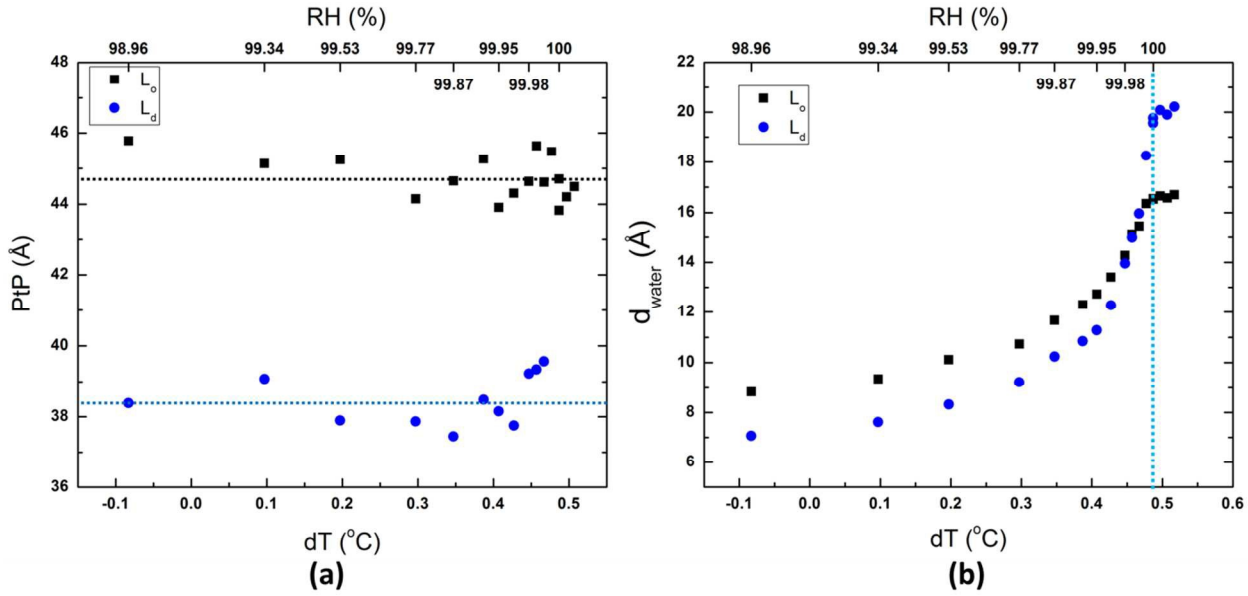

FIG. 6. (a) PtP distance of the Lo phase (black squares) and the Ld phase (blue dots) vs. RH (dT). The dotted horizontal line marks the average value. (b) Calculated water thickness vs. RH (upper scale) and dT (lower scale). The black squares represent the Lo phase while the blue dots represent the Ld phase. The vertical blue dotted line marks the 100% RH point, where the d-spacings for both phases saturate at the maximum value.

From the plot, we can see that at partial hydration of 98.96% RH, the water layer thickness of the L_d phase is about 1 Å smaller than that of the L_o phase, while somewhere close to 99.95% RH, the water spacing of the L_d phase starts to increase faster, and catches up with that of the L_o phase at around 99.98% RH, and continues to swell well beyond the water thickness of the L_o phase at 100% RH by 4 Å.

To quantitatively understand this anomalous swelling phenomenon, we employed the theoretical model by Petrache *et al.* [44] and the fitting method used in our previous study [32] to simulate a normal swelling curve to compare with our data. In a pure lipid multilayer, the water thickness between bilayers is a result of balance between the osmotic pressure of the multilayer, which is the effective combination of the Helfrich fluctuation pressure, the hydration pressure, and the van der Waals pressure:

$$P_{osm} = P_{fl} + P_h + P_{vdw} \qquad (3)$$

While the fluctuation pressure and the hydration pressure can be both approximated with exponential functions with decay length λ_{fl}, λ_h [45]

$$P_{fl} = A_{fl} e^{-a/\lambda_{fl}} \qquad (4)$$

$$P_h = A_h e^{-\frac{a}{\lambda_h}} \qquad (5)$$

The van der Waals pressure has the following form [45] :

$$P_{vdw} = -\frac{H}{6\pi}\left(-\frac{2}{(D_B' + a)^3} + \frac{1}{(2D_B' + a)^3} + \frac{1}{a^3}\right) \qquad (6)$$

Here, H is the Hamaker constant, D_B' is the bilayer thickness and a the water thickness. $D_B' + a = d$, is the d-spacing of the multilayer.

The osmotic pressure can be converted to relative humidity using the following expression [46]

$$P_{osm} = -\left(\frac{kT}{v_w}\right)\ln(RH) \qquad (7)$$

In which $v_w = 30\text{Å}^3$ is the volume of a water molecule. The simulated normal swelling curves are plotted against our data in Figure 7, and the parameters used are shown in supplementary materials Table S1. In Figure 7(a), the d-spacing vs. RH (dT) is plotted. The black dotted line represents the simulated curve of normal swelling for the L_o phase, while the red dashed line represents that of L_d phase. The anomalous swelling amount is marked by the green double arrow. Because the change in d-spacing at close to 100% RH is very steep, we convert the RH to the osmotic pressure and plot ln P vs. d-spacing in Figure 7(b) for better visualization and analysis. The blue dots represent the data for the L_d phase, while the black squares represent the data of the L_o phase. The normal swelling simulation curve is represented by the corresponding solid lines. The vertical blue dashed line marks the saturation d-spacing of the L_d phase, while the black dashed line marks the saturation d-spacing of the L_o phase, which actually is not displayed on the plot because of the divergent behavior of ln P at 100% RH. It shows clearly how the data of the L_d phase deviates from the

normal swelling curve when the system approaches full hydration.

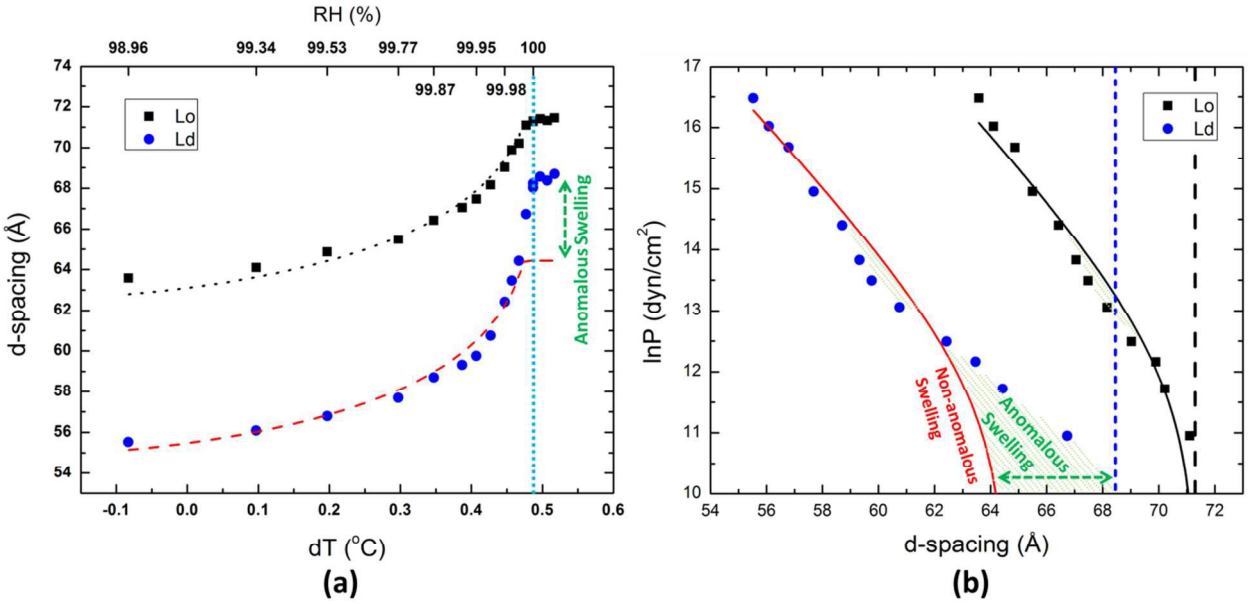

FIG. 7. The simulated normal swelling curves plotted together with anomalous swelling data. (a) The d-spacing vs. RH (dT) plot. The bottom red dashed curve represents the normal swelling curve for the Ld phase, while the top black dotted curve represents the normal swelling curve for the Lo phase. The 100% RH is marked by the vertical blue dotted line. (b) The natural log of the osmotic pressure is plotted vs. d-spacing for the same simulated normal swelling curve and anomalous swelling data. The vertical blue short dashed line marks the saturation d-spacing of the Ld phase, while the black dashed line marks the saturation d-spacing of the Lo phase.

In order to differentiate from the thermal anomalous swelling discovered by Hønger *et al.* [17] the gel-fluid phase transition, we may call this phenomenon anomalous swelling type II. This swelling occurs with phase separated mixture multilayers which have hydrophobic mismatches at the domain boundaries. Comparing with normal swelling, the difference in the d-spacings between the two phases is reduced from 7 Å to 3 Å with anomalous swelling type II.

DISCUSSION

To better visualize the anomalous swelling type II, we look back to the schematic drawing in Figure 1. Figure 1(a) represents the 99% humidity structure when the water layer thicknesses for both phases are ~8 Å. The water forms a continuous layer between the two phases to eliminate the hydrophobic mismatch energy, but the two phases will go out of phase fairly quickly, and the domain boundary has to re-adjust itself in the form of defects or extra bending with associated lipid tilt. In either form, this costs energy. The cost of energy is directly proportional to the thickness of the water layer: as RH increases, the water layer swells, therefore more mismatch energy builds up. This would explain the deviation of data from the simulation curve at ln P = 13.5 dyne/cm^2 in Figure 7(b) in both the L_d and the L_o phase, as the system is trying to reduce the free energy by suppressing the swelling. After a certain point, the mismatch energy is too big and the swelling cannot be suppressed further, the system has to restructure to reduce the free energy, and thus the anomalous swelling in the L_d phase appears. We can see that in Figure 1(b), the excess swelling of the L_d phase would close the gap between the d-spacing differences, therefore effectively reducing the mismatch energy at the domain boundary. (A brief calculation of the boundary hydrophobic mismatch energy as a function of d-spacing difference is included in the supplementary material.)

As shown in the microscope pictures in Figure 3, the in-plane domain sizes are on the order of 100 μm, which are very large domain areas. The fact that we observe only a single value of the d-spacing for each phase in the anomalous swelling state rather than a super-position of a range of d-spacings shows that the boundary effects on the swelling are quite long-range.

Associated Content

Supporting Information. Part 1. Figure S1: Optical microscopy, bright field microscopy and fluorescence microscopy pictures of phase separated ternary mixture lipid multilayer domains. Part 2. Table S1: Simulation parameters of the non-anomalous swelling curve of L_d phase and L_o phase. Part 3. Calculation of the mismatch energy with a simplified model.

Acknowledgements

X-ray data were collected on beamline 33BM at the Ad-vanced Photon Source, Argonne National Laboratory. Use of the Advanced Photon Source was supported by the U. S. Department of Energy, Office of Science, Office of Basic Energy Sciences, under Contract No. DE-AC02-06CH11357.

This work was supported by the Office of Basic Energy Sciences, U.S. Dept. of Energy under DOE Grant number: DE-FG02-04ER46173.

Notes and References

[a] Department of Physics, University of California-San Diego, La Jolla, CA-92093, USA
[b] Advanced Photon Source, Argonne National Laboratory, Argonne. IL-60439, USA
[c] Department of Physics, Northern Illinois University, DeKalb, IL-60115, USA
[*] Current Address: Department of Physics, Shiv Nadar University Chithera, Dadri, Gautam Budh Nagar, UP 203207, India
[**] Current Address: Amity University-UP, Sector-125, Noida, India
† Corresponding Author. Email: ssinha@physics.ucsd.edu

1 H. I. Petrache, N. Gouliaev, S. Tristram-Nagle, R. Zhang, R. M. Suter and J. F. Nagle, *Phys. Rev. E*, 1998, **57**, 7014–7024.
2 E. A. Evans and V. A. Parsegian, *Proc. Natl. Acad. Sci.*, 1986, **83**, 7132–7136.
3 H. I. Petrache, T. Zemb, L. Belloni and V. A. Parsegian, *Proc. Natl. Acad. Sci.*, 2006, **103**, 7982–7987.
4 H. I. Petrache, S. Tristram-Nagle, D. Harries, N. Kučerka, J. F. Nagle and V. A. Parsegian, *J. Lipid Res.*, 2006, **47**, 302–309.
5 M. A. Johnson, S. Seifert, H. I. Petrache and A. C. Kimble-Hill, *Langmuir*, 2014, **30**, 9880–9885.
6 M. M. Koerner, L. A. Palacio, J. W. Wright, K. S. Schweitzer, B. D. Ray and H. I. Petrache, *Biophys. J.*, 2011, **101**, 362–369.
7 E. Evans and D. Needham, *J. Phys. Chem.*, 1987, **91**, 4219–4228.
8 E. Sackmann, *Can. J. Phys.*, 1990, **68**, 999–1012.
9 C. M. DeCaro, J. D. Berry, L. B. Lurio, Y. Ma, G. Chen, S. Sinha, L. Tayebi, A. N. Parikh, Z. Jiang and A. R. Sandy, *Phys. Rev. E*, 2011, **84**, 041914.
10 S. Tristram-Nagle, H. I. Petrache, R. M. Suter and J. F. Nagle, *Biophys. J.*, 1998, **74**, 1421–1427.
11 M. L. Wagner and L. K. Tamm, *Biophys. J.*, 2000, **79**, 1400–1414.
12 O. Purrucker, A. Förtig, R. Jordan and M. Tanaka, *ChemPhysChem*, 2004, **5**, 327–335.
13 M. L. Wagner and L. K. Tamm, *Biophys. J.*, 2001, **81**, 266–275.
14 M. A. Deverall, E. Gindl, E.-K. Sinner, H. Besir, J. Ruehe, M. J. Saxton and C. A. Naumann, *Biophys. J.*, 2005, **88**, 1875–1886.
15 M. A. Deverall, S. Garg, K. Lüdtke, R. Jordan, J. Rühe and C. A. Naumann, *Soft Matter*, 2008, **4**, 1899–1908.
16 L. K. Tamm and H. M. McConnell, *Biophys. J.*, 1985, **47**, 105–113.
17 T. Hønger, K. Mortensen, J. Ipsen, J. Lemmich, R. Bauer and O. Mouritsen, *Phys. Rev. Lett.*, 1994, **72**, 3911–3914.
18 J. Lemmich, K. Mortensen, J. Ipsen, T. Hønger, R. Bauer and O. Mouritsen, *Phys. Rev. Lett.*, 1995, **75**, 3958–3961.
19 N. Chu, N. Kučerka, Y. Liu, S. Tristram-Nagle and J. F. Nagle, *Phys. Rev. E*, 2005, **71**, 041904.
20 G. Pabst, J. Katsaras, V. A. Raghunathan and M. Rappolt, *Langmuir*, 2002, **19**, 1716–1722.
21 P. Mason, J. Nagle, R. Epand and J. Katsaras, *Phys. Rev. E*, 2001, **63**, 030902.
22 H. Seto, N. L. Yamada, M. Nagao, M. Hishida and T. Takeda, *Eur. Phys. J. E*, 2008, **26**, 217–223.
23 S. S. Korreman and D. Posselt, *Eur. Phys. J. E*, 2000, **1**, 87–91.
24 N. Kučerka, M.-P. Nieh, J. Pencer, T. Harroun and J. Katsaras, *Curr. Opin. Colloid Interface Sci.*, 2007, **12**, 17–22.
25 L. Tayebi, Y. Ma, D. Vashaee, G. Chen, S. K. Sinha and A. N. Parikh, *Nat. Mater.*, 2012, **11**, 1074–1080.
26 S. L. Veatch and S. L. Keller, *Biophys. J.*, 2003, **85**, 3074–3083.
27 S. L. Veatch and S. L. Keller, *Phys. Rev. Lett.*, 2002, **89**, 268101.
28 S. L. Veatch and S. L. Keller, *Phys. Rev. Lett.*, 2005, **94**, 148101.
29 S. L. Veatch, K. Gawrisch and S. L. Keller, *Biophys. J.*, 2006, **90**, 4428–4436.
30 C. Li, D. Constantin and T. Salditt, *J. Phys. Condens. Matter*, 2004, **16**, S2439–S2453.
31 Y. Ma, S. K. Ghosh, D. A. DiLena, S. Bera, L. B. Lurio, A. N. Parikh and S. K. Sinha, **Manuscript submitted for publication.**
32 Y. Ma, S. K. Ghosh, S. Bera, Z. Jiang, S. Tristram-Nagle, L. B. Lurio and S. K. Sinha, *Phys. Chem. Chem. Phys.*, 2015, **17**, 3570–3576.
33 D. Marsh, *Biochim. Biophys. Acta BBA - Biomembr.*, 2009, **1788**, 2114–2123.
34 G. I. King, R. E. Jacobs and S. H. White, *Biochemistry (Mosc.)*, 1985, **24**, 4637–4645.
35 A. E. Blaurock, *J. Mol. Biol.*, 1971, **56**, 35–52.

36 W.-C. Hung, M.-T. Lee, F.-Y. Chen and H. W. Huang, *Biophys. J.*, 2007, **92**, 3960–3967.
37 S. K. Ghosh, S. Aeffner and T. Salditt, *ChemPhysChem*, 2011, **12**, 2633–2640.
38 N. P. Franks and W. R. Lieb, *J. Mol. Biol.*, 1979, **133**, 469–500.
39 S. Tristram-Nagle, H. I. Petrache and J. F. Nagle, *Biophys. J.*, 1998, **75**, 917–925.
40 J. F. Nagle and S. Tristram-Nagle, *Biochim. Biophys. Acta BBA - Rev. Biomembr.*, 2000, **1469**, 159–195.
41 H. I. Petrache, S. Tristram-Nagle and J. F. Nagle, *Chem. Phys. Lipids*, 1998, **95**, 83–94.
42 T. Salditt, *J. Phys. Condens. Matter*, 2005, **17**, R287–R314.
43 W.-C. Hung, M.-T. Lee, F.-Y. Chen and H. W. Huang, *Biophys. J.*, 2007, **92**, 3960–3967.
44 H. I. Petrache, N. Gouliaev, S. Tristram-Nagle, R. Zhang, R. M. Suter and J. F. Nagle, *Phys. Rev. E*, 1998, **57**, 7014–7024.
45 J. N. Israelachvili, *Intermolecular and Surface Forces: Revised Third Edition*, Academic Press, 2011.
46 R. P. Rand and V. A. Parsegian, *Biochim. Biophys. Acta BBA - Rev. Biomembr.*, 1989, **988**, 351–376.

